RSC Advances

PAPER

View Article Online
View Journal | View Issue

Cite this: *RSC Adv.*, 2022, **12**, 24037

High molecular weight PE elastomers through 4,4-difluorobenzhydryl substitution in symmetrical α-diimino-nickel ethylene polymerization catalysts†

Yuting Zheng, [ab] Shu Jiang, [ab] Ming Liu, [b] Zhixin Yu,*[a] Yanping Ma, [bc] Gregory A. Solan,*[bc] Wenjuan Zhang, [bd] Tongling Liang [b] and Wen-Hua Sun *[b]

The following family of *N*,*N*-diaryl-2,3-dimethyl-1,4-diazabutadienes, ArN=C(Me)C(Me)=NAr (Ar = 2,6-Me_2-4-{$CH(4\text{-}FC_6H_4)_2$}C_6H_2 **L1**, 2-Me-6-Et-4-{$CH(4\text{-}FC_6H_4)_2$}C_6H_2 **L2**, 2,4-{$CH(4\text{-}FC_6H_4)_2$}$_2$-6-MeC_6H_2 **L3**, 2,4-{$CH(4\text{-}FC_6H_4)_2$}$_2$-6-EtC_6H_2 **L4**, 2,4-{$CH(4\text{-}FC_6H_4)_2$}$_2$-6-$iPrC_6H_2$ **L5**), each incorporating *para*-substituted 4,4-difluorobenzhydryl groups but differing in the *ortho*-pairing, have been synthesized and used as precursors to their respective nickel(II) bromide complexes, **Ni1–Ni5**. Compound characterization has been achieved through a combination of FT-IR, multinuclear NMR spectroscopy (^{1}H, ^{13}C, ^{19}F) and elemental analysis. In addition, **L1**, **Ni1** and **Ni5** have been structurally characterized with **Ni1** and **Ni5** revealing similarly distorted tetrahedral geometries about nickel but with distinct differences in the steric protection offered by the *ortho*-substituents. All nickel complexes, under suitable activation, showed high activity for ethylene polymerization with a predilection towards forming branched high molecular weight polyethylene with narrow dispersity. Notably the most sterically bulky **Ni5**, under activation with either $EtAlCl_2$, Et_2AlCl or EASC, was exceptionally active (0.9–1.0 × 10^7 g of PE per (mol of Ni) per h) at an operating temperature of 40 °C. Furthermore, the polyethylene generated displayed molecular weights close to one million g mol^{-1} (M_w range: 829–922 kg mol^{-1}) with high branching densities (86–102/1000 carbons) and a selectivity for short chain branches (% Me = 94.3% ($EtAlCl_2$), 87.2% (Et_2AlCl), 87.7% (EASC)). Further analysis of the mechanical properties of the polymers produced at 40 °C and 50 °C using **Ni5** highlighted the key role played by crystallinity (X_c) and molecular weight (M_w) on tensile strength (σ_b) and elongation at break (ε_b). In addition, stress–strain recovery tests reveal these high molecular weight polymers to exhibit characteristics of thermoplastic elastomers (TPEs).

Received 13th July 2022
Accepted 17th August 2022

DOI: 10.1039/d2ra04321a

rsc.li/rsc-advances

Introduction

The synthesis of late transition-metal catalysts for ethylene polymerization has remained a subject of enduring interest in academia and industry, since the groundbreaking work by Brookhart and co-workers on α-diimine group 10 (nickel and palladium) catalysts in the mid-1990s.[1–3] Perhaps more remarkable is the fact that these highly active catalysts can allow the formation of moderate to highly branched polymers by using ethylene as the single feedstock.[4] Since then, this catalyst class has been the target of a multitude of studies[1a,3,5] with variations in the steric[6] and electronic properties[5b,7] of the ligand frame allowing a means to regulate and control the performance of the catalyst and the structural properties of the polyethylene.

With particular regard to α-diimino-nickel catalysts, great advances have been made over the last few years with regard to improvements in thermal stability and catalytic activity of their active species. These developments have largely been concerned with modifying the ligand backbone and changing the substituents on the imino *N*-aryl groups.[3c] In terms of our contribution to the area, we have examined in some depth the scope of non-symmetric 1,2-bis(imino)acenaphthene-nickel(II) halide complexes (**A**, Chart 1), where one *N*-aryl group is appended with sterically bulky benzhydryl ($CHPh_2$) or its fluorinated derivatives, *e.g.*, Ar[1] = 2,6-dibenzhydryl-4-R,[8] 2,6-bis(di-fluorobenzhydryl)-4-R,[9] 2,4-dibenzhydryl-6-R[10] and 2,4-

[a]*School of Pharmaceutical Sciences, Changchun University of Chinese Medicine, Changchun 130117, China. E-mail: yuzx01@ccucm.edu.cn*

[b]*Key Laboratory of Engineering Plastics, Beijing National Laboratory for Molecular Sciences, Institute of Chemistry, Chinese Academy of Sciences, Beijing 100190, China. E-mail: gas8@leicester.ac.uk; whsun@iccas.ac.cn*

[c]*Department of Chemistry, University of Leicester, University Road, Leicester LE1 7RH, UK*

[d]*Beijing Key Laboratory of Clothing Materials R&D and Assessment, Beijing Engineering Research Center of Textile Nanofiber, School of Materials Science and Engineering, Beijing Institute of Fashion Technology, Beijing 100029, China*

† Electronic supplementary information (ESI) available: NMR spectra of ligand compounds and complexes, GPC traces of polyethylenes, and crystal data and structure refinements along with X-ray crystallographic data. CCDC 2161608 (**L1**), 2161609 (**Ni1**) and 2161610 (**Ni5**). For ESI and crystallographic data in CIF or other electronic format see https://doi.org/10.1039/d2ra04321a

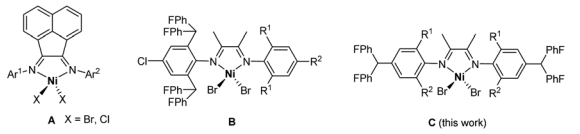

Chart 1 α-Diimino-nickel(II) halide complexes based on unsymmetrical 1,2-bis(arylimino)acenaphthenes (**A**) and 2,3-dimethyl-1,4-diazabutadienes (**B**) along with target precatalyst, **C**.

bis(difluorobenzhydryl)-6-R[11] (R = alkyl, halide and aryl). As a result, certain conclusions can be drawn from these investigations, including the increased thermostability of these catalysts and the enhanced catalytic activity, particularly for the 4,4-difluorobenzhydryl-substituted systems; polyethylenes generated can vary from low molecular weight to narrowly dispersed high molecular weight. From our viewpoint, these fundamental studies can help accelerate the synthesis of an industrially relevant α-diimine catalyst that can achieve precise regulation of the polymer.

By the same token, *N*,*N*′-diaryl-2,3-dimethyl-1,4-diazabutadiene-nickel complexes (**B**, Chart 1) incorporating 2,6-bis(difluorobenzhydryl) groups on one side of the ligand frame, have shown encouraging results by producing highly branched polyethylene with high molecular weight that can sometimes display bimodal distributions.[12] As with the **A**-type precatalysts, the presence of the fluoro-substituents has been demonstrated to have a beneficial effect on both catalytic activity as well as on the thermal stability.

As part of our current program, we are aiming to expand the types of nickel catalyst by harnessing the positive influence of the 4,4-difluorobenzhydryl groups on catalytic activity and other properties.[9,11] In particular, we report herein a new series of symmetrical *N*,*N*-diaryl-2,3-dimethyl-1,4-diazabutadiene-nickel precatalysts (**C**, Chart 1), that all contain one *para*-4,4-difluorobenzhydryl substituent per *N*-aryl group but differ in the pairings for the *ortho*-substituents ((Me/Me, Me/Et, Me/(*p*-FPh)$_2$CH), Et/(*p*-FPh)$_2$CH, iPr/(*p*-FPh)$_2$CH). We considered that this progressive increase in the steric properties of the *ortho*-substitution pattern would not only impact on catalytic activity and thermostability, but also on the polymer molecular weight and the degree and composition of branching. The control of the latter being central to the development of elastomeric polyethylene with high molecular weight.[13] Consequently, a thorough ethylene polymerization study is described to explore these changes, and also probe the influence of co-catalyst type, run temperature and ethylene pressure. All ligands and complexes are new and so full details for ligand synthesis and complexation are reported. Furthermore, the potential for isomeric species in the ligand, precatalyst and catalyst offers additional points of interest.

Results and discussion

Synthesis and characterization of L1–L5 and Ni1–Ni5

The *N*,*N*-diaryl-2,3-dimethyl-1,4-diazabutadienes, ArN=C(Me)C(Me)=NAr, where Ar = 2,6-Me$_2$-4-{CH(4-FC$_6$H$_4$)$_2$}C$_6$H$_2$ **L1**, 2-Me-6-Et-4-{CH(4-FC$_6$H$_4$)$_2$}C$_6$H$_2$ **L2**, 2,4-{CH(4-FC$_6$H$_4$)$_2$}$_2$-6-MeC$_6$H$_2$ **L3**, 2,4-{CH(4-FC$_6$H$_4$)$_2$}$_2$-6-EtC$_6$H$_2$ **L4**, 2,4-{CH(4-FC$_6$H$_4$)$_2$}$_2$-6-iPrC$_6$H$_2$ **L5**), were prepared in two steps (Scheme 1). Firstly, 2,3-butanedione was treated with the corresponding 4,4-difluorobenzhydryl-substituted aniline in acetic acid in the presence of zinc(II) chloride. The resulting zinc intermediate was then demetallated by interaction with an aqueous solution of potassium carbonate to afford **L1–L5**; similar template/demetallation approaches have been reported previously.[14] All α-diimines were characterized by ^{1}H NMR and ^{13}C NMR spectroscopy (see Fig. S1–S10†), FT-IR spectroscopy (see Fig. S11–S15†) and elemental analysis. Subsequently, reacting **L1–L5** with (DME)NiBr$_2$ (DME = 1,2-dimethoxyethane) in THF at ambient temperature gave on work-up, [(ArN=C(Me)C(Me)=NAr)]NiBr$_2$ (Ar = 2,6-Me$_2$-4-{CH(4-FC$_6$H$_4$)$_2$}C$_6$H$_2$ **Ni1**, 2-Me-6-Et-4-{CH(4-FC$_6$H$_4$)$_2$}C$_6$H$_2$ **Ni2**, 2,4-{CH(4-FC$_6$H$_4$)$_2$}$_2$-6-MeC$_6$H$_2$ **Ni3**, 2,4-{CH(4-FC$_6$H$_4$)$_2$}$_2$-6-EtC$_6$H$_2$ **Ni4**, 2,4-{CH(4-FC$_6$H$_4$)$_2$}$_2$-6-iPrC$_6$H$_2$ **Ni5**), in good yield (Scheme 1). All complexes were isolated as air stable brick red solids and characterized by FT-IR spectroscopy (see Fig. S16–S20†), ^{1}H NMR (see Fig. S21–S25†) and ^{19}F NMR spectroscopy (see Fig. S26–S30†) and elemental analysis. In addition, the molecular structures of **L3**, **Ni1** and **Ni5** were determined by single crystal X-ray diffraction.

Several isomers are possible for **L1–L5** on the basis of *Z*,*E*-isomerism about the C=N bonds, *s-cis*/*s-trans* isomerism and *anti*/*syn* isomerism as a result of hindered rotation of the *N*-aryl groups (Scheme 2).[5g,h,j,6c,15] Given that **L2** (R^1 = Me, R^2 = Et) shows peaks for one compound in its ^{1}H NMR spectrum (see Fig. S2†), it would suggest that *E*,*E*/*Z*,*E* and *s-cis*/*s-trans* interconversions for both **L2**-*anti* and **L2**-*syn* are fast on the laboratory timescale at room temperature. By contrast for **L3–L5**, two isomers were seen in their ^{1}H NMR spectra in ratios of approximately 5 : 1 which we have attributed to the presence of *anti* and *syn* isomers, respectively (see Fig. S3–S5†). In these cases the steric properties of the sterically bulky *ortho*-CH(*p*-FPh)$_2$ groups are considered to impede *N*-aryl rotation resulting in an enriched *anti* conformer. Similar observations are seen in the fluorine-free comparators of **L3–L5**.[5k] The ^{1}H NMR spectra of the complexes were all broad and paramagnetically shifted (*S* = 1) (see Fig. S21–S25†). For example, the ^{1}H NMR spectrum of **Ni4** displayed two broad signals around δ_H 24 and δ_H 28 ppm for its *ortho*-ethyl groups due to its steric hindrance[16] (see Fig. S24†). By comparison for **Ni2**, at least three broad resonances are observed in the δ_H 24–28 ppm region **Ni2** (see

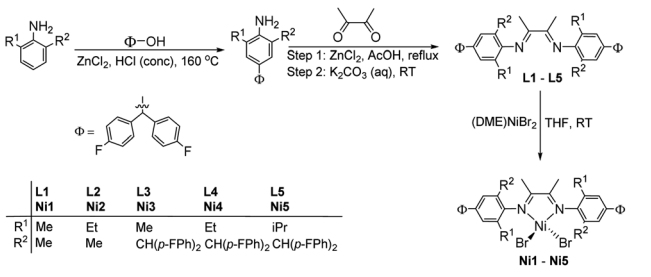

Scheme 1 Synthetic route to the *N*,*N*-diaryl-2,3-dimethyl-1,4-diazabutadienes (**L1–L5**) and their nickel(II) bromide complexes (**Ni1–Ni5**).

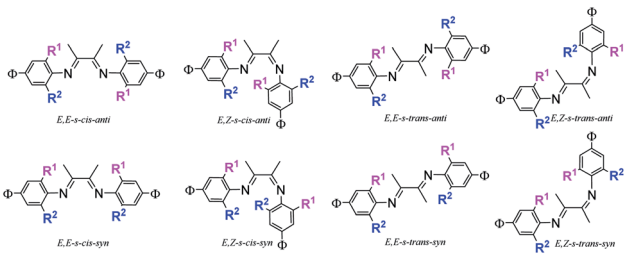

Scheme 2 Some possible isomers for **L1–L5** based on *E*/*Z* isomerism, *s-cis*/*s-trans* isomerism and *anti*/*syn* isomerism; where ϕ = CH(*p*-FPh)$_2$.

Fig. S22†), which would suggest the presence of both **Ni2**-*anti* and **Ni2**-*syn* forms. Similar phenomena were seen in the ^{1}H NMR spectra of **Ni3–Ni5** (see Fig. S14 and S25†), which were likely due to the characteristic temperature dependence and relaxation effects of paramagnetic complexes.[16,17]

In the ^{19}F NMR spectrum of **L1** a single broad peak at δ −116.85 ppm was seen on account of the equivalent *para*-4,4-difluorobenzhydryl groups, which is slightly downfield shifted on coordination to nickel (see Fig. S26a† for spectra of **L1** and **Ni1**). By contrast in **L3**, the ^{19}F NMR spectrum showed three distinct fluoride resonances, two closely located signals at δ −116.69 and −116.80 ppm, and another more downfield at δ −115.87 ppm. By comparison with **L1**, the more intense resonance at δ −116.69 can be assigned to the freely rotating *para*-4,4-difluorobenzhydryl groups, while the other two resonances to inequivalent CH(4-FC$_6$H$_4$)$_a$(4-FC$_6$H$_4$)$_b$ groups on account of restricted rotation due to the proximity of the imine-methyl group,[18] further evidence for this restricted rotation can be detected in the ^{13}C NMR spectra (see Fig. S5–S10†). Similarly, complex **Ni3** display three fluoride resonances in an approximate 1 : 2 : 1 ratio (Fig. 1b and S28†), with the signals at δ −114.44 and δ −116.38 ppm assignable to the *ortho*-CH(4-FC$_6$H$_4$)$_a$(4-FC$_6$H$_4$)$_b$ groups, while the third resonance centered at δ −115.33 ppm to the *para*-4,4-difluorobenzhydryl substituent. Closer inspection of this latter signal, however, reveals it to comprise two closely located resonances, which would suggest that some restricted C$_{para}$-aryl rotation is also possible in the complex. Notably, in **Ni4** these signals for the *para*-CH(4-FC$_6$H$_4$)$_a$(4-FC$_6$H$_4$)$_b$ groups become more distinct (Fig. S29†).

Single crystals of **L3**, **Ni2** and **Ni5** of appropriate quality for the X-ray determination were obtained by layering dichloromethane solutions of each compound with diethyl ether. The structures of **L3**, **Ni1** and **Ni5** are depicted in Fig. 2–4, while selected bond lengths and angles are collected in Table 1. For **Ni5** two independent molecules (A and B) were present in the asymmetric unit while in **L3** there were three (A, B and C). As the molecules showed only minimal differences, only molecule A for each structure will be discussed in any detail. For the two nickel complexes, **Ni1** and **Ni5**, the structures are similar and based on a four coordinate nickel center bound by a bidentate *N*,*N*-diaryl-2,3-dimethyl-1,4-diazabutadiene ligand (aryl = 2,6-dimethyl-4-bis(4-fluorophenyl)methylphenyl **Ni1** and 2,4-di{bis(4-fluorophenyl)methyl}-6-isopropylphenyl **Ni5**) and two monodentate bromide ligands. In terms of geometry, this can be described as distorted tetrahedral which is in part enforced by the N–Ni–N bite angle of the *N*,*N*-chelating ligand [81.2(3)° **Ni1**, 81.7(3)° **Ni5**]. Notably, there is some variation in the Br1–Ni1–Br2 angles between the two structures (123.15(9)° **Ni1**, 116.69(9)° **Ni5**), which may relate to the differences in substitution pattern on the *N*-aryl groups. The Ni–N bond lengths in both structures are comparable [Ni(1)–N(1) 2.024(8) Å (**Ni1**), 2.009(9) Å (**Ni5**); Ni(1)–N(2) 2.006(9) Å (**Ni1**), 2.014(8) Å (**Ni5**)], as are the Ni–Br lengths [Ni(1)–Br(1) 2.338(2) Å (**Ni1**), 2.336(2) Å (**Ni5**); Ni(1)–Br(2) 2.317(2) Å (**Ni1**), 2.326(2) Å (**Ni5**)] and indeed consistent with that found in previous reports.[8a,19–22] The planes of the *N*-aryl groups are almost perpendicular to the coordination plane C3–C4–N1–Ni–N2, as evidenced by the dihedral angles for **Ni1** (83.25°, 88.55°) and **Ni5** (81.20°, 78.94°). By comparison, the structure of the free ligand, **L3**, shows a *E*,*E*-*s*-*trans* configuration with the bulky *ortho*-substituents on each *N*-aryl ring adopting an *anti* conformer; such a transoid disposition of the imine nitrogens in 1,4-diazabutadienes is commonplace.[15] The C–N$_{imine}$ bond lengths (N1–C3 1.276(3) Å, N2–C4 1.270(3) Å) are nonetheless similar to that seen in complexes **Ni1** (N1–C3 1.288(13) Å, N2–C4 1.323(12) Å) and **Ni5** (N1–C3 1.291(12) Å, N2–C4 1.286(12) Å). The 4,4-difluorobenzhydryl substituents in each of the three structures show no unusual features.

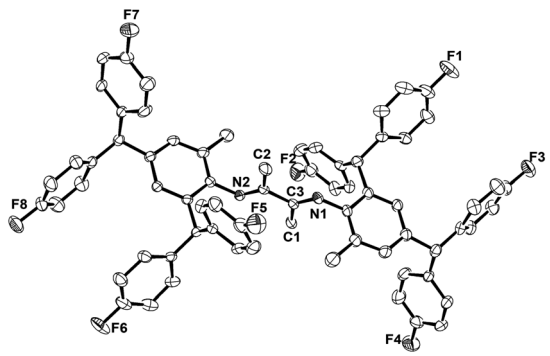

Fig. 1 ORTEP drawing of **L3** (molecule A). Thermal ellipsoids are shown at the 30% probability level while the hydrogen atoms have been omitted for clarity.

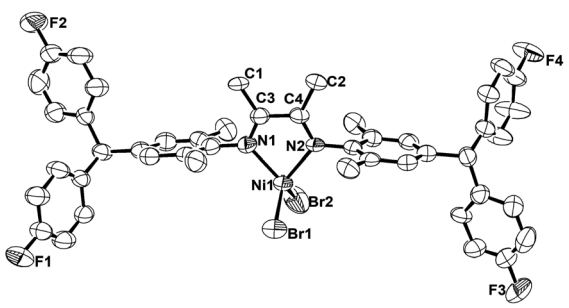

Fig. 2 ORTEP drawing of **Ni1**. Thermal ellipsoids are shown at the 30% probability level while the hydrogen atoms have been omitted for clarity.

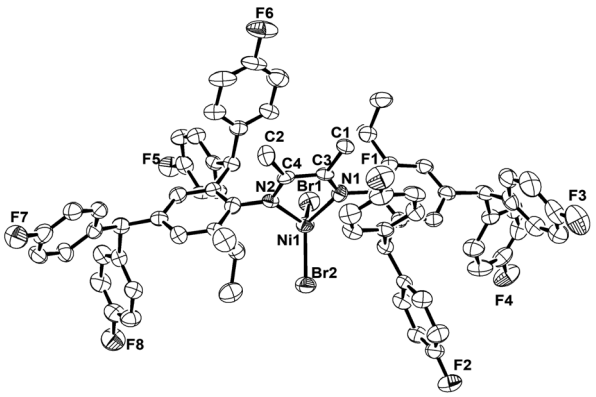

Fig. 3 ORTEP drawing of **Ni5** (molecule A). Thermal ellipsoids are shown at the 30% probability level while the hydrogen atoms have been omitted for clarity.

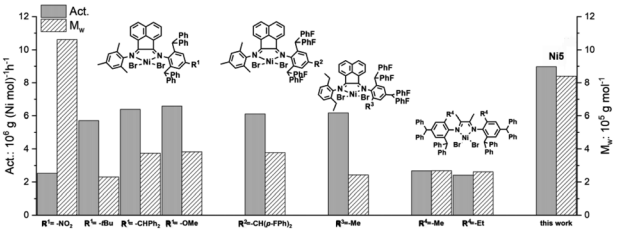

Fig. 4 Comparison of catalytic activity and molecular weight of the PE produced using **Ni5** with that for $A_{2,6\text{-}(CHPh_2)_2}$, $A_{2,6\text{-}\{(p\text{-}FPh)_2CH\}_2}$, $A_{2,4\{(p\text{-}FPh)_2CH\}2}$ and fluorine-free examples of $C_{2,4(CHPh_2)_2}$; all polymerizations performed in toluene at 40 °C under similar conditions using Et_2AlCl as co-catalyst.

Ethylene polymerization evaluation

Co-catalyst screen. In the first instance, we set about identifying the most suitable co-catalyst to deliver the highest productivity by employing 2-methyl-6-ethyl-4-{bis-(4,4-difluorobenzhydryl)}phenyl substituted **Ni2** as our test pre-catalyst. Five commonly employed aluminum-alkyl co-catalysts were initially explored namely, methylaluminoxane (MAO), modified MAO (MMAO; contains 20–25% Al^iBu_3), diethylaluminum chloride (Et_2AlCl), ethylaluminum dichloride ($EtAlCl_2$) and ethylaluminum sesquichloride (EASC). All preliminary polymerization runs were performed in toluene at 30 °C with the ethylene pressure kept at 10 atm and the run time at 30 minutes; the results of the evaluations are collected in Table 2. Inspection of the data reveals that all the aluminum alkyls were capable of activating **Ni2** with MAO the standout performer allowing **Ni2** to reach the maximum activity of 6.84×10^6 g of PE per (mol of Ni) per h. On the basis of the level of catalytic activity, MAO was taken forward for further investigation as was $EtAlCl_2$ which proved the second most effective co-catalyst (5.21×10^6 g of PE per (mol of Ni) per h).

Ethylene polymerization using Ni1–Ni5 in combination with MAO

To allow an optimization of the performance of **Ni2**/MAO and in turn establish a set of conditions that could be utilized to screen the other nickel precatalysts, we initiated a study to explore the

Table 2 Screening of **Ni2** for ethylene polymerization with a selection of different co-catalysts[a]

Entry	Co-cat.	Al : Ni	Activity[b]	M_w[c]	M_w/M_n[c]	T_m[d] (°C)
1	MAO	2000	6.84	2.25	2.27	105.5
2	MMAO	2000	4.11	2.53	2.62	112.4
3	$EtAlCl_2$	400	5.21	2.53	2.55	104.4
4	Et_2AlCl	400	4.81	1.91	2.72	106.3
5	EASC	400	4.08	2.34	3.12	106.8

[a] General conditions: 2 μmol of **Ni2**, 30 °C, 30 min, 10 atm ethylene, 100 mL toluene. [b] $\times 10^6$ g of PE per (mol of Ni) per h. [c] Determined by GPC, M_w in units of $\times 10^5$ g mol^{-1}. [d] Determined by DSC.

Table 1 Selected bond lengths (Å) and angles (°) for **L3**, **Ni1** and **Ni5**

	L3 (molecule A)	**Ni1**	**Ni5** (molecule A)
Br(1)–Ni(1)	—	2.336(2)	2.338(2)
Br(2)–Ni(1)	—	2.326(2)	2.317(2)
Ni(1)–N(1)	—	2.009(9)	2.007(8)
Ni(1)–N(2)	—	2.014(8)	2.019(7)
N(1)–C(3)	1.276(3)	1.288(13)	1.291(12)
N(2)–C(4)	1.270(3)	1.323(12)	1.286(12)
N(1)–C(5)	1.413(2)	1.433(12)	1.413(13)
C(4)–C(3)	1.502(3)	1.493(14)	1.498(14)
C–F (range)	1.352(3)-1.364(2)	1.349(13)-1.376(13)	1.359(14)-1.381(15)
Br(2)–Ni(1)–Br(1)	—	123.15(9)	116.69(9)
N(2)–Ni(1)–Br(1)	—	116.4(2)	116.4(2)
N(2)–Ni(1)–Br(2)	—	109.2(2)	109.2(2)
N(1)–Ni(1)–Br(1)	—	100.4(3)	100.4(3)
N(1)–Ni(1)–Br(2)	—	118.6(2)	118.6(2)
N(1)–Ni(1)–N(2)	—	81.7(3)	81.7(3)
C(4)–C(3)–N(1)	115.97(19)	117.0(8)	116.6(8)
C(3)–C(4)–N(2)	115.45(10)	114.6(8)	115.0(8)

effect of Al : Ni molar ratio, run time, temperature and ethylene pressure; the complete set of results are gathered in Table 3.

With the temperature maintained at 30 °C, the Al : Ni molar ratio using **Ni2**/MAO was subject to a stepwise increase from 1000 : 1 to 3000 : 1 (entries 1–5, Table 3). Initially the activity was seen to rise reaching a highpoint of 7.17×10^6 g of PE per (mol of Ni) per h with the ratio at 1500 : 1, then as the ratio was increased further the activity progressively decreased. As a further point, the activity was seen to increase sharply when the Al : Ni molar ratio was adjusted from 1000 : 1 to 1500 : 1, which suggests there is a critical amount of MAO required before good activity can be achieved. As has been previously observed, the amount of MAO employed can influence the molecular weight of the polymer.[9a–c,11,12,19,22–24] Similarly in this case, an increase in the Al : Ni molar ratio led to a decrease in the value of M_w from 539 kg mol^{-1} at 1000 : 1 to 186 kg mol^{-1} at 3000 : 1 (Fig. S32†). It would seem likely that termination of the polymerization involving chain transfer to aluminum is to some extent operational with larger ratios of MAO.[8b,f,9d,11] Some support for this is provided by the absence of detectable downfield vinylic peaks in the δ 110 − 140 region (Fig. S40†) of the ^{13}C NMR spectrum of the polymer (see later), although the high molecular weight of this polymer may also explain this absence.

With the Al : Ni molar ratio retained at 1500 : 1, the polymerization runs using **Ni2**/MAO were performed at five distinct temperatures ranging from 20 °C to 60 °C. Examination of the data revealed that at 30 °C, the activity of 7.17×10^6 g of PE per (mol of Ni) per h remained the highest (entry 2, Table 3). It was apparent that on raising the temperature beyond 30 °C, the rate of chain transfer increased while the active species showed some evidence of deactivation.[25] Meanwhile, the influence of temperature on the molecular weight of the polymer was similar than that seen with a change in the Al : Ni molar ratio. In particular, on raising the temperature of the run, the molecular weight of the polymer decreased from 614 kg mol^{-1} at 20 °C to 100 kg mol^{-1} at 60 °C (Fig. S33†); a finding that can be attributed to thermally induced chain transfer.[8b,f,9d,10a,11]

With the temperature and the amount of MAO retained at 30 °C and 1500 equivalents, respectively, the impact of run time on the performance of **Ni2**/MAO was explored. By employing set times between 5 minutes and 60 minutes (entries 2, 10–13, Table 3), it was noted that the peak activity was observed after 5 minutes with levels reaching up to 15.6×10^6 g of PE per (mol of Ni) per h. Such a highpoint in activity early in the run would imply rapid formation of the active species followed by gradual catalyst deactivation.[6c] Nonetheless, even after one hour, the activity still remained at an appreciable level [3.94×10^6 g of PE per (mol of Ni) per h] highlighting the significant lifetime displayed by this catalyst. Further studies showed that the response of **Ni2**/MAO to variations in ethylene pressure were consistent with previous studies,[19] with a lowering in the pressure leading to a reduction in the activity (entries 14 and 15, Table 3). Concomitantly, the molecular weight of the polymer decreased, and the dispersity broadened. It would seem plausible that a reduced ethylene pressure would result in mass transport limitations of the ethylene monomer leading to an increase in the rate of chain transfer to aluminum, thereby decreasing the molecular weight of the polymer.[6c,8g]

With an effective set of reaction conditions now established for **Ni2**/MAO, the remaining precatalysts, **Ni1**, **Ni3–Ni5**, were then evaluated similarly with the aim to explore the influence of structural changes to the ligand frame on catalytic performance (entries 16–19, Table 3). All catalysts displayed good activity ($1.13–7.17 \times 10^6$ g of PE per (mol of Ni) per h) generating polymers that showed narrow dispersities (M_w/M_n range: 2.18–2.88). Overall, the order of activity was as follows: **Ni2** [2-Me-6-Et-4-(4,4-difluorobenzhydryl)] > **Ni1** [2,6-Me$_2$-4-(4,4-difluorobenzhydryl)] > **Ni3** [2,4-di(4,4-difluoro-benzhydryl)-6-Me] > **Ni4** [2,4-di(4,4-difluorobenzhydryl)-6-Et] > **Ni5** [2,4-di(4,4-difluorobenzhydryl)-6-iPr].

Several points emerge from inspection of this order. Firstly, the precatalysts incorporating the less sterically bulky *ortho*-substituents, **Ni1** (Me/Me) and **Ni2** (Me/Et) proved the most active, which is consistent with previous observations.[21] Of these two systems, **Ni2** showed the highest productivity [7.17×10^6 g of PE per (mol of Ni)], which may originate from favorable electronic or steric factors imparted by the possible *syn*/*anti* conformers; this is, however, far from clear.[5g,6,7] Secondly, it is apparent that the incorporation of one sterically bulky *ortho*-(4,4-difluorobenzhydryl) group per *N*-aryl unit depressed activity at this temperature. It is possible that the *anti*/*syn* mixture seen in **L3–L5**, may not in this case be beneficial to the polymerization if reproduced in **Ni3–Ni5**. Nonetheless, for the three catalysts based on this substitution pattern (**Ni3**, **Ni4** and **Ni5**), the

Table 3 Results for the ethylene polymerization evaluation using **Ni1–Ni5** in combination with MAO[a]

Entry	Precat.	T (°C)	t (min)	Al : Ni	Act.[b]	M_w[c]	M_w/M_n[c]	T_m[d] (°C)
1	**Ni2**	30	30	1000	1.12	5.39	2.59	127.6
2	**Ni2**	30	30	1500	7.17	3.13	2.58	107.5
3	**Ni2**	30	30	2000	6.84	2.25	2.27	105.2
4	**Ni2**	30	30	2500	6.12	2.14	2.44	116.0
5	**Ni2**	30	30	3000	5.76	1.86	2.68	111.3
6	**Ni2**	20	30	1500	1.05	6.14	2.34	129.6
7	**Ni2**	40	30	1500	3.56	2.25	2.77	121.5
8	**Ni2**	50	30	1500	2.48	1.80	2.20	118.7
9	**Ni2**	60	30	1500	1.02	1.00	3.06	93.4
10	**Ni2**	30	5	1500	15.60	2.31	2.73	116.5
11	**Ni2**	30	15	1500	11.84	3.12	2.14	113.3
12	**Ni2**	30	45	1500	5.11	3.18	2.00	124.9
13	**Ni2**	30	60	1500	3.94	4.05	2.92	126.4
14[e]	**Ni2**	30	30	1500	2.77	2.42	2.43	121.1
15[f]	**Ni2**	30	30	1500	0.08	0.71	5.51	65.4
16	**Ni1**	30	30	1500	6.01	9.11	2.88	111.3
17	**Ni3**	30	30	1500	3.93	9.42	2.18	116.6
18	**Ni4**	30	30	1500	1.54	3.63	2.75	116.9
19	**Ni5**	30	30	1500	1.13	10.48	2.37	95.5
20	**Ni5**	40	30	1500	3.17	8.67	2.49	68.1
21	**Ni5**	50	30	1500	1.01	7.44	2.65	63.1

[a] General conditions: 2 μmol of nickel precatalyst, 30 °C, 30 min, 10 atm ethylene, 100 mL toluene. [b] $\times 10^6$ g of PE per (mol of Ni) per h. [c] Determined by GPC, M_w in units of $\times 10^5$ g mol^{-1}. [d] Determined by DSC. [e] 5 atm of ethylene. [f] 1 atm of ethylene.

steric properties of the second *ortho*-substituent (Me, Et, iPr) proved influential with 6-methyl **Ni3** more active than 6-isopropyl **Ni5**.

By contrast, in terms of polymer molecular weight the order follows: **Ni5** [2,4-di(4,4-difluorobenzhydryl)-6-iPr] > **Ni3** [2,4-di(4,4-difluorobenzhydryl)-6-Me] > **Ni1** [2,6-Me_2-4-(4,4-difluorobenzhydryl)] > **Ni4** [2,4-di(4,4-difluorobenzhydryl)-6-Et] > **Ni2** [2-Me-6-Et-4-(4,4-difluorobenzhydryl)]. Interestingly, for *ortho*-ethyl substituted **Ni2** and **Ni4**, the molecular weight of the resulting polymers was notably lower than that seen with the other catalysts (M_w range: 313–363 kg mol^{-1}). However, it remains unclear as to how this structural variation makes it more amenable to chain transfer.[6c,8g] On the other hand, the molecular weight of the polymer produced using the most sterically bulky **Ni5** was more than a million g mol^{-1} (*i.e.*, 1048 kg mol^{-1}, entry 19, Table 3); see Fig. S30† for a pictorial representation of the molecular weight variations. Notably, when compared with their non-fluorinated benzhydryl comparators,[21,26] these MAO-activated *para*-4,4-difluorobenzhydryl-substituted nickel complexes exhibited higher activities (see later). Such a finding is consistent with the electron-withdrawing fluoride substituents enhancing the Lewis acidity of the active metal species leading to more effective monomer coordination and insertion.[27–29]

To probe the response of *ortho*-(4,4-difluorobenzhydryl)-substituted **Ni5** to run temperature, we also investigated **Ni5**/MAO at temperatures in excess of 30 °C. Significantly, this catalyst almost trebled its level of activity when the temperature was raised to 40 °C (3.17×10^6 g of PE per (mol of Ni) per h), a finding that underlines the capacity of the bulky *ortho*-CH(4-$FC_6H_4)_2$ group to improve the thermal stability of the catalyst. A plausible explanation can be attributed to the increased spatial volume present at the *ortho*-position leading to an enhanced shielding effect on the axial positions in the active nickel catalyst, thus inhibiting the chain transfer.[1a,4a]

Ethylene polymerization using Ni1–Ni5 in combination with $EtAlCl_2$

With the intention to explore the influence of co-catalyst on the performance of the nickel precatalyst and in turn the properties of the polymers generated, we then undertook a more in-depth evaluation using $EtAlCl_2$ as the co-catalyst. As with the MAO investigation, **Ni2** was selected as the trial precatalyst and an optimization of the Al : Ni molar ratio, temperature, time and ethylene pressure re-conducted; the results are documented in Table 4.

As with the **Ni2**/MAO study, **Ni2**/$EtAlCl_2$ was first investigated at 30 °C with the Al : Ni molar ratio in this case adjusted from 300 : 1 to 800 : 1 (entries 1–6, Table 4). The results revealed that the peak activity of 6.48×10^6 g of PE per (mol of Ni) per h was achieved at 600 : 1 which compares with 7.17×10^6 g of PE per (mol of Ni) per h for **Ni2**/MAO. However, and unlike that seen for **Ni2**/MAO, the molecular weight of the polyethylene can be more precisely controlled with values typically around 200 kg mol^{-1} (M_w range: 205–263 kg mol^{-1}), with significantly less influence caused by changing the amount of alkylaluminum.

Table 4 Results for the ethylene polymerization evaluation using **Ni1–Ni5** in combination with $EtAlCl_2$[a]

Entry	Precat.	T (°C)	t (min)	Al : Ni	Act.[b]	M_w[c]	M_w/M_n[c]	T_m[d] (°C)
1	**Ni2**	30	30	300	3.28	2.34	2.87	107.7
2	**Ni2**	30	30	400	5.21	2.53	2.55	104.4
3	**Ni2**	30	30	500	5.83	2.48	2.59	106.3
4	**Ni2**	30	30	600	6.48	2.05	2.79	99.0
5	**Ni2**	30	30	700	4.84	2.63	2.05	110.1
6	**Ni2**	30	30	800	4.24	2.48	2.31	112.7
7	**Ni2**	20	30	600	5.30	3.64	2.73	116.5
8	**Ni2**	40	30	600	5.82	1.18	1.96	87.9
9	**Ni2**	50	30	600	4.88	1.03	2.36	86.5
10	**Ni2**	60	30	600	2.39	0.69	2.76	65.0
11	**Ni2**	30	5	600	17.52	1.49	2.76	108.3
12	**Ni2**	30	15	600	7.40	1.87	2.46	112.7
13	**Ni2**	30	45	600	4.74	2.27	2.72	108.7
14	**Ni2**	30	60	600	3.73	2.40	2.56	109.5
15[e]	**Ni2**	30	30	600	4.93	1.60	2.43	106.7
16[f]	**Ni2**	30	30	600	0.35	0.68	1.91	47.8
17	**Ni1**	30	30	600	6.14	13.08	2.17	109.9
18	**Ni3**	30	30	600	7.43	8.19	2.84	109.0
19	**Ni4**	30	30	600	4.95	1.28	2.90	114.0
20	**Ni5**	30	30	600	4.81	15.19	2.30	93.3
21	**Ni5**	40	30	600	9.20	9.22	2.45	69.6
22	**Ni5**	50	30	600	4.43	8.88	2.25	50.1
23[g]	**Ni5**	40	30	600	8.97	8.36	2.68	77.3
24[h]	**Ni5**	40	30	600	10.03	8.29	3.12	73.8

[a] General conditions: 2 μmol of nickel precatalyst, 30 °C, 30 min, 10 atm ethylene, 100 mL toluene. [b] $\times 10^6$ g of PE per (mol of Ni) per h. [c] Determined by GPC, M_w in units of $\times 10^5$ g mol^{-1}. [d] Determined by DSC. [e] 5 atm of ethylene. [f] 1 atm of ethylene. [g] **Ni5** in combination with Et_2AlCl. [h] **Ni5** in combination with EASC.

This finding would also suggest that the larger amounts of co-catalyst required in the MAO runs to allow effective pre-catalyst activation, also facilitated more effective chain transfer to MAO.[8b,f,9d,11]

As for the effect of run temperature, the activity of **Ni2**/$EtAlCl_2$ and the molecular weight of the resulting polymer showed similar variations to that seen with **Ni2**/MAO (entries 4, 7–10, Table 4). Indeed, **Ni2**/$EtAlCl_2$ also reached its maximum activity at 30 °C (6.48×10^6 g of PE per (mol of Ni) per h), but the increase in level from that noted at 20 °C (5.30×10^6 g of PE per (mol of Ni) per h) was less pronounced. Evidently, lower temperature can hinder the activation of **Ni2** with MAO. Furthermore, **Ni2**/$EtAlCl_2$ at 60 °C still maintained an appreciable level of activity (2.39×10^6 g of PE per (mol of Ni) per h) which by comparison is more than double that seen for **Ni2**/MAO (1.02×10^6 g of PE per (mol of Ni) per h) at the same temperature.

Likewise, the response to run time for **Ni2**/$EtAlCl_2$ was similar to that found for **Ni2**/MAO with the former attaining its maximum activity after 5 minutes [17.52×10^6 g of PE per (mol of Ni) per h] and thereafter decreasing to 3.73×10^6 g of PE per (mol of Ni) per h at 60 minutes with the onset of catalyst deactivation. Nonetheless, the molecular weight gradually increased over time implying the presence of sufficient active species to sustain chain propagation (entries 4, 11–14, Table 4).

On reducing the ethylene pressure of the run to 5 atm and then 1 atm saw the activity of **Ni2**/$EtAlCl_2$ drop and the resulting molecular weight of the polymer fall; related findings has been reported in previous literature.[9a,23b]

As a common feature of the polymers generated during the optimization process for **Ni2**/$EtAlCl_2$ was their narrow dispersity (M_w/M_n range: 1.91–2.87). Indeed, a similar observation was made with **Ni2**/MAO, which highlights the single-site nature of these catalysts and in turn the good control imparted on propagation. On the other hand, and as a notable difference, the molecular weight of the polymers produced by **Ni2**/MAO (M_w range: 100–614 kg mol^{-1}) was in general higher when compared to that seen for **Ni2**/$EtAlCl_2$ (M_w range: 69–364 kg mol^{-1}) (*vide infra*).

Subsequently, we subjected **Ni1**, **Ni3**, **Ni4** and **Ni5**, to the optimized conditions established for **Ni2**/$EtAlCl_2$ (Al : Ni molar ratio = 600 : 1, T = 30 °C, run time = 30 min). All five pre-catalysts including **Ni2** showed good activity spanning the range, 4.81–7.43 × 10^6 g of PE per (mol of Ni) per h (*cf.* 1.13–7.17 × 10^6 g of PE per (mol of Ni) per h for MAO). With respect to the relative performance, this order was: **Ni3** [2,4-di(4,4-difluorobenzhydryl)-6-Me] > **Ni2** [2-Me-6-Et-4-(4,4-difluorobenzhydryl)] > **Ni1** [2,6-Me_2-4-(4,4-difluorobenzhydryl)] > **Ni4** [2,4-di(4,4-difluorobenzhydryl)-6-Et] > **Ni5** [2,4-di(4,4-difluorobenzhydryl)-6-iPr]. Scrutiny of this downward trend highlights one key difference to that seen with MAO : **Ni3**, incorporating a sterically bulky *ortho*-substituent, is now the most active system of the series (7.43 × 10^6 g of PE per (mol of Ni) per h, entry 18, Table 4), rather than in third place as was seen with MAO. The main reason behind this observation remains unclear but it may be derive from the different binding capacities between the active nickel center and aluminum-based anion in the active species.[30,31]

In terms of the molecular weight of the polymers generated, these fell in a wider range than with MAO [M_w range: 128–1519 kg mol^{-1} ($EtAlCl_2$) *vs.* 313–1048 kg mol^{-1} (MAO)] with the highest molecular weight material significantly greater with $EtAlCl_2$. Pertaining to the precatalyst, the value of M_w falls in the order: **Ni5** [2,4-di(4,4-difluorobenzhydryl)-6-iPr] > **Ni1** [2,6-Me_2-4-(4,4-difluorobenzhydryl)] > **Ni3** [2,4-di(4,4-difluorobenzhydryl)-6-Me] > **Ni2** [2-Me-6-Et-4-(4,4-difluorobenzhydryl)] ∼ **Ni4** [2,4-di(4,4-difluorobenzhydryl)-6-Et]. In the main, this order resembles that seen with MAO with the most sterically bulky precatalyst **Ni5** forming the highest molecular weight polymer, while *ortho*-ethyl containing **Ni2** and **Ni4**, the lowest. Indeed, **Ni5**/$EtAlCl_2$ is amenable to forming ultra-high molecular weight polyethylene (UHMWPE) with the run temperature at 30 °C; see Fig. S34† for a depiction of these trends. As with the MAO study, the reason why the *ortho*-ethyl-containing precatalysts (**Ni2** and **Ni4**) have a tendency to form lower molecular weight polymer remains unclear; we nevertheless consider this a valuable feature for catalyst design.

As with **Ni5**/MAO, we also explored the performance of **Ni5**/$EtAlCl_2$ at run temperatures of greater than 30 °C. Significantly, at 40 °C a dramatic increase in activity was observed with **Ni5**/$EtAlCl_2$ reaching a value of 9.20 × 10^6 g of PE per (mol of Ni) per h that equates to a 90% improvement in activity; even at 50 °C the level only dropped to 4.43 × 10^6 g of PE per (mol of Ni) per h (*cf.* MAO for 3.17 × 10^6 g of PE per (mol of Ni) per h at 40 °C and 1.01 × 10^6 g of PE per (mol of Ni) per h at 50 °C). Evidently, both **Ni5**/MAO and **Ni5**/$EtAlCl_2$ show heightened performance characteristics at higher run temperature which is particular true for $EtAlCl_2$, which evidently reflects the enhanced thermal stability of the active species formed with this co-catalyst. Though numerous publications of the use of 2,3-dimethyl-1,4-diazabutadiene-nickel precatalysts in ethylene polymerization have been reported,[1g,3b,4,5f,12,13,19–21,26] relatively few have been concerned with the generation of polyethylene elastomers at higher run temperature. However in those cases, the elastomeric materials tend to be of too low a molecular weight. It is noteworthy that with the current modification to the *N*,*N*-ligand frame, the catalyst, **Ni5**/$EtAlCl_2$, displays not only enhanced thermal stability, but also produces polyethylene elastomers displaying amongst the highest molecular weights (9.22 × 10^5 g mol^{-1} at 40 °C and 8.88 × 10^5 g mol^{-1} at 50 °C).

In order to further probe the outstanding performance characteristics displayed by **Ni5** at higher temperature, we extended the investigation to include two other aluminum-alkyl co-catalysts namely EASC and Et_2AlCl (entries 23 and 24, Table 4). While **Ni5**/Et_2AlCl showed similar performance to **Ni5**/$EtAlCl_2$ (entry 21 *vs.* 23, Table 4), the activity of **Ni5**/EASC reached an exceptional level of 1.0 × 10^7 g of PE per (mol of Ni) per h at 40 °C (entry 24, Table 4), which is to the knowledge of the authors among one the highest reported for α-diimine-nickel complexes operating at this temperature. Furthermore, the molecular weight of the polyethylene obtained using both **Ni5**/Et_2AlCl and **Ni5**/EASC remained exceptionally high. To illustrate these results, Fig. 4 collects together catalytic activity and polymer molecular weight data for **Ni5**/Et_2AlCl alongside that produced using selected examples of **A** (Chart 1) as well as fluorine-free analogues of the current precatalysts **C**;[8b–g,9b,11,21] all catalytic runs were performed under comparable conditions and co-catalyst. As a further point that can be gleaned from inspection of this figure, it is apparent that the introduction of electron-withdrawing fluoro-substituents in **Ni5** enhances catalytic activity, findings that are consistent with previously reported experimental observations[9,11] and calculations.[27–29]

Properties of the polyethylenes

^{13}C NMR spectroscopic studies. On the basis of the high catalytic activity displayed by **Ni2**/MAO at 30 °C (entry 2, Table 3) together with **Ni5**/$EtAlCl_2$, **Ni5**/Et_2AlCl and **Ni5**/EASC at 40 °C (entries 21, 23 and 24, Table 4), the structural properties of the resulting polymers, PE-M30Ni2, PE-$EtAlCl_2$40Ni5, PE-Et_2-AlCl40Ni5 and PE-EASC40Ni5, were investigated by ^{13}C NMR spectroscopy. To allow suitable solubility, these four polymer samples were dissolved at 100 °C in either chlorobenzene-d_5 or *o*-dichlorobenzene-d_4 and their spectra recorded at this temperature (Fig. S40–S43†); the assignment of the spectra was based on approaches documented in the literature (Table 5).[32]

On examination of the results, it is apparent that all four polyethylene samples contain a significant amount of

Table 5 Branching density and composition of the PEs[a,b]

PE sample	Branches/1000Cs	Branching composition (%)						
		Me	Et	Pr	Bu	Amyl	Me (1,4-paired)	Me (1,6-paired)
PE-M30Ni2	50	70.9	3.22	3.04	6.30	2.79	4.39	4.76
PE-EtAlCl$_2$40Ni5	86	81.6	1.17	0.07	2.50	0.68	6.58	5.63
PE-Et$_2$AlCl40Ni5	86	75.9	1.90	1.43	2.67	1.51	5.76	5.51
PE-EASC40Ni5	102	72.2	3.09	1.39	2.64	1.52	7.92	7.60

[a] Data obtained using ^{13}C NMR spectroscopy. [b] Analysis performed using approaches described in ref. 32.

branching that would be expected on the basis of a chain walking mechanism.[33] Notably, the polymers obtained using **Ni5**/EtAlCl$_2$, **Ni5**/Et$_2$AlCl and **Ni5**/EASC displayed a higher degree of branching than that seen with **Ni2**/MAO and also contain a greater amount of short chain branching (>87%); the lower values of T_m also reflects this (see Tables 3 and 4).[34,35] This would suggest that the steric hindrance provided by the difluorobenzhydryl groups likely inhibits extensive "chain-walking" and favors monomer insertion; the difference in run temperature may also be a contributing factor. It has been reported in previous experiments that higher polymerization temperatures result in more highly branched polyethylene.[3b,5b,c,10b,24,26] Based on literature precedent, we propose the methyl branch is generated by a single chain walking step involving β-H elimination, a 2,1-reinsertion and then coordination/insertion of ethylene. In the current system, the steric hindrance imparted by the *ortho*-alkyl group inhibits further nickel migration to a more bulky secondary Ni-alkyl resulting in high levels of methyl branches. Unlike the results by Gao and co-workers,[33e] the presence of methyl branches was not accompanied by sizable amounts of long chain branching. Evidently, the current catalysts allow good control of the type of branch which will likely impact on the performance characteristics of these polyethylene materials (see later). Meanwhile, it is evident that the type of aluminum activator exerts some effect on the branching density of the polyethylene (EASC > Et$_2$AlCl ∼ EtAlCl$_2$) with EASC preferring to form more highly branched polyethylene. This finding is consistent with recent work in our group concerning EASC-activated α-diimino-nickel complexes in ethylene polymerization.[8f]

Mechanical properties of the polyethylenes

In order to assess the mechanical properties of the branched polyethylenes generated using **Ni5** at higher run temperature (40–50 °C), we selected six samples prepared using this pre-catalyst but differing in the co-catalyst and temperature: PE-40MNi5 (entry 20, Table 3), PE-50MNi5 (entry 21, Table 3), PE-40EtAlCl$_2$Ni5 (entry 21, Table 4), PE-50EtAlCl$_2$Ni5 (entry 22, Table 4), PE-Et$_2$AlCl40Ni5 and PE-EASC40Ni5. Each sample was subjected to a tensile stress–strain test using a universal tester and a stress–strain recovery test using dynamic mechanical analysis (DMA); the full set of results are given in Table 6.

Firstly, monotonic tensile stress–strain measurements were undertaken at room temperature with each test performed with three specimens in order to achieve concordant results; the stress–strain curves are depicted in Fig. 5. For the two samples prepared using EtAlCl$_2$, PE-EtAlCl$_2$40Ni5 displayed the higher crystallinity (X_c = 20.06%), molecular weight (922 kg mol^{-1}) and ultimate tensile strength (6.5 MPa), while the strain at break (223%) was lower. By comparison the maximum value of elongation at break was observed for PE-E50Ni5 (413%), while the level of crystallinity (X_c = 13.60%) and molecular weight (888 kg mol^{-1}) were less. Similar observations were noted for the two samples prepared with **Ni5**/MAO, with PE-M40Ni5 showing the higher tensile stress [σ_b = 10.06 MPa], crystallinity [X_c = 22.4%] and molecular weight [M_w = 867 kg mol^{-1}] but with the lower strain at break [ε_b = 366%]. Clearly the degree of crystallinity impacts on the mechanical properties of these polymers,[36] with higher crystallinity leading to polyethylene displaying the highest ultimate tensile strength but the lower value of ε_b. Nonetheless, the variations in molecular weight of the polymers should also likely impact on these mechanical properties. Furthermore, by consideration of the four polymer samples obtained at 40 °C, it apparent that the type of aluminum co-catalyst also impacts on the mechanical properties with stress-at-break values ranging from 4.6 to 10.06 MPa and strain-at-break values ranging from 211% to 382%. As a final point, PE-M50Ni5 displayed a higher tensile stress and a reasonable elongation at break when compared with polymers obtained in previous work using nickel catalysts under similar conditions (*i.e.*, MAO as activator, reaction temperature = 50 °C, $P_{C_2H_4}$ = 10 atm and run time = 30 min).[9a,b]

Secondly, the six polyethylene samples were subjected to stress–strain recovery tests by using dynamic mechanical

Table 6 Selected properties of the PE samples obtained using **Ni5** with various co-catalysts and run temperatures

PE sample	T, °C	T_m[a], °C	M_w[b]	X_c[a], %	σ_b[c], MPa	ε_b, %
PE-EtAlCl$_2$40Ni5	40	69.6	9.22	20.06	6.5	223
PE-EtAlCl$_2$50Ni5	50	50.1	8.88	13.60	4.0	413
PE-M40Ni5	40	68.0	8.67	22.40	10.06	366
PE-M50Ni5	50	63.1	7.44	16.96	5.41	405
PE-Et$_2$AlCl40Ni5	40	77.3	8.36	16.30	5.62	211
PE-EASC40Ni5	40	73.8	8.29	15.71	4.60	382

[a] Determined by DSC; $X_c = \Delta H_f(T_m)/\Delta H_f^\circ(T_m^\circ)$; $\Delta H_f^\circ(T_m^\circ) = 248.3$ J g^{-1}. [b] Determined by GPC, values ×10^5 g mol^{-1}. [c] Determined by using a universal tester.

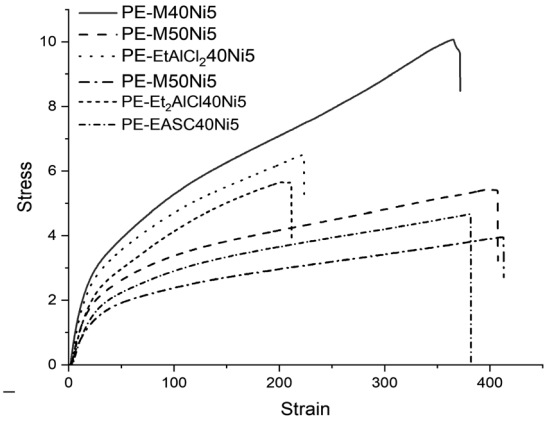

Fig. 5 Stress–strain curves for samples, PE-$EtAlCl_2$40Ni5, PE-$EtAlCl_2$50Ni5, PE-M40Ni5, PE-M50Ni5, PE-Et_2AlCl40Ni5 and PE-EASC40Ni5; the vertical line represents the breakage point.

analysis at 30 °C (Fig. S44†). Ten cycles were involved in each recovery test to allow for elastic extenuation, while the elastic recovery (R) was recorded at about 80% of the maximum tensile strength (σ); σ was also determined by using dynamic mechanical analysis. The stress–strain hysteresis loops showed constant recovery levels observed for all samples after the first cycle, which demonstrated that all samples possessed the characteristics of thermoplastic elastomers (TPE's). With an increase in the polymerization run temperature from 40 °C to 50 °C, the R value of the polymer generated using $EtAlCl_2$ improved from 47.7% to 52.8%. Similarly, the elastic recovery of the sample produced using MAO increased from 46.1% to 48.0%. Evidently, this study of elastic recovery indicates that the run temperature also played an important role in the elastomeric properties of the polymer besides crystallinity. It is worth highlighting that the high molecular weight of the polymer samples described herein makes them unique when compared with previously reported polyethylenes with thermoplastic elastomer characteristics.[5l,8c,8d,g,9a]

Experimental section

General considerations

Standard Schlenk techniques were utilized under an atmosphere of nitrogen to manipulate all air- and moisture-sensitive compounds. Under nitrogen, toluene was dried over sodium metal at reflux and distilled before use. MAO (1.46 M solution in toluene), MMAO (2.00 M in n-heptane) and $EtAlCl_2$ (2.17 M in hexane) were purchased from Akzo Nobel Corp. Diethylaluminum chloride (Et_2AlCl, 1.17 M in toluene) and ethylaluminum sesquichloride (EASC, 0.87 M in toluene) were purchased from Acros Chemicals. Other reagents were purchased from Aldrich, Acros or local suppliers. High-purity ethylene was purchased from Beijing Yanshan Petrochemical Company and used as received. ^{1}H and ^{13}C NMR spectra were recorded on a Bruker DMX 400 MHz instrument and ^{19}F NMR spectra were recorded on a Bruker AVANCE III 500 MHz at ambient temperature using tetramethylsilane (TMS) as an internal standard. IR spectra were recorded on a PerkinElmer System 2000 FT-IR spectrometer. Elemental analyses were conducted using a Flash EA 1112 microanalyzer. Molecular weights (M_w) and dispersities (M_w/M_n) of polyethylene were determined by a PL-GPC220 at 160 °C with 1,2,4-trichlorobenzene as the eluting solvent. Differential scanning calorimetry (DSC) was used to measure melting points of the polyethylene; these were acquired from the second scanning run on PerkinElmer DSC-7 at a heating rate of 10 °C min^{-1}. ^{13}C NMR spectra of polymer were recorded on a Bruker AVANCE III 500 MHz instrument at 100 °C in chlorobenzene-d_5 or o-dichlorobenzene-d_4 with TMS as an internal standard. Operating conditions used for the ^{13}C NMR spectra of polymer samples, PE-MAO30Ni2 and PE-$EtAlCl_2$40Ni5: spectral width 31.250 kHz, acquisition time 0.26 s, relaxation delay 1.5 s, number of scans around 2048. Operating conditions used for the ^{13}C NMR spectra of polymer samples, PE-Et_2AlCl40Ni5 and PE-EASC40Ni5: spectral width 31.250 kHz, acquisition time 0.52 s, relaxation delay 2.0 s, number of scans around 2048. The five types of 4,4-difluorobenzhydryl-substituted aniline were synthesized using reported procedures.[37,38]

Synthesis of ArN=C(Me)C(Me)=NAr (L1–L5)

(a) Ar = 2,6-Me_2-4-{$CH(4\text{-}FC_6H_4)_2$}C_6H_2 (L1). To a 100 mL round-bottomed flask, equipped with stir bar, was added zinc(II) chloride (0.40 g, 3.0 mmol), 2,3-butanedione (0.26 g, 3.0 mmol), 2,6-dimethyl-4-bis(4-fluorophenyl)methylaniline (2.0 g, 6.0 mmol) and acetic acid (2 mL). The reaction mixture was stirred and heated for 4 h at 80 °C. Once cooled to room temperature, diethylether (10 mL) was added and the resulting yellow precipitate filtered. This intermediate zinc(II) chloride complex was then dissolved in dichloromethane and a saturated aqueous solution of potassium carbonate added and the stirred at room temperature for 1.5 h.[39–41] Using a separating funnel, the organic layer was extracted and washed with water three times and dried over $MgSO_4$. After the volatiles were removed by rotary evaporation, the product was recrystallized with hexane and washed with acetonitrile to give **L1** as a yellow powder (1.14 g, 55%). ^{1}H NMR ($CDCl_3$, 400 MHz, TMS): δ 7.07 (t, J = 5.6 Hz, 8H, Ar–H), 6.98 (t, J = 8.8 Hz, 8H, Ar–H), 6.77 (s, 4H, Ar–H), 5.44 (s, 2H, CH(p-FPh)$_2$), 2.04 (s, 6H, MeC=N), 1.98 (s, 12H, Ar–Me). ^{13}C NMR ($CDCl_3$, 100 MHz, TMS): δ 168.26 (N=CMe), 162.67 (p-FC_6H_5), 160.24 (p-FC_6H_5), 146.75, 139.95, 139.91, 138.34, 130.81, 130.73, 128.82, 124.80, 115.21, 115.00, 54.82 (CH(p-FPh)$_2$), 17.91 (CH_3), 15.97 (N=CMe). ^{19}F NMR (470 MHz, $CDCl_3$): δ −116.85. FT-IR (cm^{-1}): 2970 (w), 2914 (w), 2888 (w), 1892 (w), 1648 (m, $\nu_{C=N}$), 1599 (m), 1504 (s), 1471 (w), 1432 (w), 1382 (w), 1355 (w), 1294 (w), 1217 (s), 1155 (s), 1135(w), 1117 (w), 1095 (w), 1013 (m), 962 (w), 936 (w), 893 (w), 835 (s), 783 (m), 754 (m), 716 (w). Anal. calcd for $C_{46}H_{40}N_2$ (696.83): C, 79.29; H, 5.79; N, 4.02. Found: C, 78.89; H, 5.77; N, 3.69.

(b) Ar = 2-Me-6-Et-4-{$CH(4\text{-}FC_6H_4)_2$}C_6H_2 (L2). A similar synthetic procedure as described for **L1** but using 2-methyl-6-ethyl-4-{4,4-difluorobenzhydryl}aniline as the aniline, gave **L2** as a yellow solid (0.85 g, 41%). ^{1}H NMR ($CDCl_3$, 400 MHz, TMS): δ 7.10–7.06 (m, 8H, Ar–H), 6.99 (t, J = 8.6 Hz, 8H, Ar–H), 6.78 (d,

J = 12.7 Hz, 4H, Ar–H), 5.46 (s, 2H, CH(p-FPh)$_2$), 2.38–2.29 (m, 4H, Ar–CH_2CH_3), 2.05 (s, 6H), 1.96 (s, 6H), 1.08 (t, J = 7.5 Hz, 6H). ^{13}C NMR ($CDCl_3$, 100 MHz, TMS): δ 168.26 (N=CMe), 162.66 (p-FC_6H_5), 160.23 (p-FC_6H_5), 146.25, 140.01, 139.98, 138.45, 131.10, 131.07, 130.81, 130.73, 128.82, 127.20, 127.17, 124.48, 115.19, 114.98, 54.91 (CH(p-FPh)$_2$), 24.94 (CH_2), 24.89 (CH_2), 17.91 (CH_3), 16.15 (CH_3), 13.75 (N=CMe), 13.72 (N=CMe). ^{19}F NMR (470 MHz, $CDCl_3$): δ −116.88. FT-IR (cm^{-1}): 2968 (w), 2918 (w), 2859 (m), 1895 (w), 1655 (m, $\nu_{C=N}$), 1600 (m), 1504 (s), 1460 (w), 1425 (w), 1377 (w), 1357 (m), 1295 (w), 1219 (s), 1157 (s), 1118 (m), 1097 (w), 1016 (w), 966 (w), 934 (w), 873 (w), 832 (s), 786 (m), 757 (w), 717 (w), 639 (w). Anal. calcd for $C_{48}H_{44}N_2$ (724.89): C, 79.53; H, 6.12; N, 3.86. Found: C, 79.43; H, 6.02; N, 3.49.

(c) Ar = 2,4-{CH(4-FC_6H_4)$_2$}$_2$-6-MeC_6H_2 (L3). A similar synthetic procedure as described for **L1** but using 2,4-di{4,4-difluorobenzhydryl}-6-methylaniline gave **L3** as a yellow solid (1.16 g, 36%). ^{1}H NMR (400 MHz, $CDCl_3$): two isomers are present in a 5 : 1 ratio, δ 6.95–6.91 (m, 16H, Ar–H), 6.88–6.81 (m, 18H, Ar–H), 6.37 (s, Ar–H, integrates to 0.33H, isomer 2), 6.32 (s, Ar–H, integrates to 1.65H, isomer 1), 5.38 (s, 2H, CH(p-FPh)$_2$), 5.22 (s, CH(p-FPh)$_2$, integrates to 1.65H, isomer 1), 5.19 (s, CH(p-FPh)$_2$, integrates to 0.33H, isomer 2), 1.90 (s, MeC=N, integrates to 5H, isomer 1), 1.88 (s, MeC=N, integrates to 1H, isomer 2), 1.53 (s, Ar–Me, integrates to 1H, isomer 2) and 1.34 (s, Ar–Me, integrates to 5H, isomer 1). ^{13}C NMR ($CDCl_3$, 100 MHz, TMS): δ 168.73 (N=CMe), 162.67 (p-FC_6H_5), 162.66 (p-FC_6H_5), 162.59 (p-FC_6H_5), 160.23 (p-FC_6H_5), 160.22 (p-FC_6H_5), 160.15 (p-FC_6H_5), 146.03, 139.71, 139.68, 139.63, 139.60, 138.77, 138.41, 138.11, 138.08, 132.41, 130.78, 130.70, 130.61, 130.53, 129.54, 128.40, 124.41, 115.52, 115.31, 115.18, 115.16, 114.97, 114.95, 114.74, 54.67 (CH(p-FPh)$_2$), 50.91 (CH(p-FPh)$_2$), 50.39 (CH(p-FPh)$_2$), 17.85 (CH_3), 17.81 (CH_3), 16.37 (N=CMe), 15.97 (N=CMe). ^{19}F NMR (565 MHz, $CDCl_3$): δ −115.87, −116.69, −116.80. FT-IR (cm^{-1}): 2972 (w), 2918 (w), 2877 (w), 1892 (w), 1647 (m, $\nu_{C=N}$), 1601 (m), 1506 (s), 1467 (w), 1421 (w), 1366 (m), 1333 (w), 1300 (w), 1227 (s), 1156 (s), 1131(m), 1095 (m), 1016 (w), 943 (w), 829 (s), 785 (m), 753 (w), 717 (w), 668 (w). Anal. calcd for $C_{70}H_{52}N_2$ (1073.19): C, 78.34; H, 4.88; N, 2.16. Found: C, 78.78; H, 5.05; N, 2.08.

(d) Ar = 2,4-{CH(4-FC_6H_4)$_2$}$_2$-6-EtC_6H_2 (L4). A similar synthetic procedure as described for **L1** but using 2,4-di{4,4-difluorobenzhydryl}-6-ethylaniline gave **L4** as a yellow solid (1.35 g, 41%). ^{1}H NMR (400 MHz, $CDCl_3$): two isomers are present in a 5 : 1 ratio, δ 6.95–6.93 (m, 16H, Ar–H), 6.90–6.81 (m, 18H, Ar–H), 6.37 (s, Ar–H, integrates to 0.33H, isomer 2), 6.31 (s, Ar–H, integrates to 1.65H, isomer 1), 5.38 (s, 2H, CH(p-FPh)$_2$), 5.21(s, CH(p-FPh)$_2$, integrates to 1.65H, isomer 1), 5.17 (s, CH(p-FPh)$_2$, integrates to 0.33H, isomer 2), 2.18 (q, 4H, J = 7.2 Hz, Ar–CH_2CH_3), 1.53 (s, MeC=N, integrates to 1H, isomer 2), 1.35 (s, MeC=N, integrates to 5H, isomer 1), 1.12 (t, J = 7.5 Hz, Ar–CH_2CH_3, integrates to 5H, isomer 1), 1.03 (t, J = 7.5 Hz, Ar–CH_2CH_3, integrates to 1H, isomer 2). ^{13}C NMR ($CDCl_3$, 100 MHz, TMS): δ 168.69 (N=CMe), 162.66 (p-FC_6H_5), 162.61 (p-FC_6H_5), 162.58 (p-FC_6H_5), 160.22 (p-FC_6H_5), 160.17 (p-FC_6H_5), 160.14 (p-FC_6H_5), 145.55, 139.79, 139.75, 139.72, 139.69, 138.96, 138.93, 138.42, 138.10, 131.85, 130.76, 130.68, 130.61, 130.59, 130.58, 130.53, 130.52, 130.28, 128.60, 128.40, 127.71, 127.42, 115.48, 115.37, 115.26, 115.15, 114.94, 114.92, 114.71, 54.79 (CH(p-FPh)$_2$), 50.89 (CH(p-FPh)$_2$), 50.40 (CH(p-FPh)$_2$), 24.49 (CH_2), 23.97 (CH_2), 16.57 (CH_3), 16.21 (CH_3), 13.66 (N=CMe), 13.43 (N=CMe). ^{19}F NMR (470 MHz, $CDCl_3$): δ −115.86, −116.72, −116.84. FT-IR (cm^{-1}): 3038 (w), 2969 (w), 2877 (w), 1894 (w), 1643 (m, $\nu_{C=N}$), 1601 (m), 1505 (s), 1450 (w), 1420 (w), 1363 (w), 1307 (w), 1225 (s), 1156 (s), 1125 (m), 1094 (w), 1014(w), 940 (w), 900 (w), 830 (s), 787 (m), 750 (w), 718 (w), 668 (w). Anal. calcd for $C_{72}H_{56}N_2$ (1101.24): C, 78.53; H, 5.13; N, 2.54. Found: C, 78.68; H, 5.26; N, 2.29.

(e) Ar = 2,4-{CH(4-FC_6H_4)$_2$}$_2$-6-iPrC_6H_2 (L5). A similar synthetic procedure as described for **L1** but using 2,4-di{4,4-difluorobenzhydryl}-6-isopropylaniline gave **L5** as a yellow solid (1.45 g, 43%). ^{1}H NMR (400 MHz, $CDCl_3$): two isomers are present in a 5 : 1 ratio, δ 6.95–6.92 (m, 16H, Ar–H), 6.91–6.80 (m, 18H, Ar–H), 6.33 (s, Ar–H, integrates to 0.33H, isomer 2), 6.28 (s, Ar–H, integrates to 1.65H, isomer 1), 5.38 (s, 2H, CH(p-FPh)$_2$), 5.18 (s, CH(p-FPh)$_2$, integrates to 1.65H, isomer 1), 5.15 (s, CH(p-FPh)$_2$, integrates to 0.33H, isomer 2), 2.52–2.40 (m, 2H, Ar–$CH(CH_3)_2$), 1.58 (s, MeC=N, integrates to 1H, isomer 2), 1.35 (s, MeC=N, integrates to 5H, isomer 1), 1.15 (d, J = 6.9 Hz, Ar–$CHMe_2$, integrates to 5H, isomer 1), 1.02 (d, J = 6.8 Hz, Ar–$CHMe_2$, integrates to 1H, isomer 2). ^{13}C NMR (100 MHz, $CDCl_3$) δ 168.78 (N=CMe), 162.64 (p-FC_6H_5), 162.62 (p-FC_6H_5), 162.57 (p-FC_6H_5), 160.21 (p-FC_6H_5), 160.17 (p-FC_6H_5), 160.13 (p-FC_6H_5), 144.81, 139.86, 139.82, 139.77, 139.74, 139.06, 139.03, 138.45, 138.10, 138.07, 135.34, 135.12, 131.62, 130.76, 130.68, 130.59, 130.52, 128.48, 128.32, 125.00, 115.43, 115.22, 115.14, 114.93, 114.90, 114.68, 54.88 (CH(p-FPh)$_2$), 50.99 (CH(p-FPh)$_2$), 50.53 (CH(p-FPh)$_2$), 28.37 (–$CH(CH_3)_2$), 27.88 (–$CH(CH_3)_2$), 23.86 (CH_3), 23.09 (CH_3), 22.63 (CH_3), 22.30 (CH_3), 16.77 (N=CMe), 16.48(N=CMe). ^{19}F NMR (470 MHz, $CDCl_3$): δ −115.85, −116.75, −116.85. FT-IR (cm^{-1}): 3039 (w), 2969 (w), 2873 (w), 1895 (w), 1643 (m, $\nu_{C=N}$), 1601 (m), 1505 (s), 1452 (w), 1420 (w), 1363 (m), 1300 (w), 1225 (s), 1156 (s), 1125 (m), 1095 (w), 1015 (w), 962 (w), 940 (w), 903 (w), 830 (s), 787 (m), 750 (w), 718 (w), 668 (w). Anal. calcd for $C_{74}H_{60}N_2$ (1129.30): C, 79.53; H, 6.12; N, 3.86. Found: C, 79.64; H, 6.22; N, 3.54.

Synthesis of [ArN=C(Me)C(Me)=NAr]$NiBr_2$ (Ni1–Ni5)

(a) Ar = 2,6-Me_2-4-{CH(4-FC_6H_4)$_2$}C_6H_2 (Ni1). All complexes were prepared based using the following procedure.[19] A Schlenk tube equipped with a stir bar was evacuated and transferred to the glove box. The tube was then back-filled with nitrogen and **L1** (0.10 g, 0.16 mmol) and (DME)$NiBr_2$ (0.05 g, 0.15 mmol) introduced to the tube. Tetrahydrofuran (3 mL) was added and the mixture left to stir overnight at room temperature. The solvent was removed under reduced pressure and diethyl ether added to induce precipitation. This solid was filtered and washed three times with a mixture of dichloromethane and diethyl ether to give **Ni1** as a brick red solid (0.106 g, 76%). ^{19}F NMR (470 MHz, $CDCl_3$): δ −115.58. FT-IR (cm^{-1}): 3043 (w), 2962 (w), 2913 (w), 1895 (w), 1639 (m, $\nu_{C=N}$), 1602 (m), 1505 (s), 1473 (w), 1413 (w), 1375 (w), 1300 (w), 1223 (s), 1157 (s), 1097 (w), 1013 (w), 896 (w), 829 (s), 780 (m), 753 (m), 722 (w), 688 (w). Anal.

calcd for $C_{46}H_{40}N_2$ (915.34): C, 60.36; H, 4.40; N, 3.06. Found: C, 59.96; H, 4.41; N, 3.02.

(b) Ar = 2-Me-6-Et-4-{CH(4-FC$_6$H$_4$)$_2$}C$_6$H$_2$ (Ni2). By employing a similar approach to that described for **Ni1** but using **L2** as the a-diimine, **Ni2** was isolated as a brick red complex (0.108 g, 79%). ^{19}F NMR (470 MHz, $CDCl_3$): δ −115.64. FT-IR (cm^{-1}): 2970 (w), 2913 (w), 2875 (m), 1892 (w), 1644 (m, $\nu_{C=N}$), 1601 (m), 1505 (s), 1462 (w), 1413 (w), 1375 (w), 1295 (w), 1222 (s), 1157 (s), 1096 (w), 1013 (w), 988 (w), 902 (w), 835 (s), 782 (w), 748 (w), 683 (w). Anal. calcd for $C_{48}H_{44}N_2$ (943.39): C, 61.11; H, 4.70; N, 2.97. Found: C, 61.52; H, 4.49; N, 2.59.

(c) Ar = 2,4-{CH(4-FC$_6$H$_4$)$_2$}$_2$-6-MeC$_6$H$_2$ (Ni3). By employing a similar approach to that described for **Ni1** but using **L3** as the a-diimine, **Ni3** was isolated as a brick red complex (0.147 g, 76%). ^{19}F NMR (470 MHz, $CDCl_3$): δ −114.44, −115.32, −115.34, −116.38. FT-IR (cm^{-1}): 3069 (w), 2911 (w), 2861 (w), 1902 (w), 1635 (m, $\nu_{C=N}$), 1601 (m), 1505 (s), 1468 (w), 1439 (w), 1413 (m), 1378 (w), 1300 (w), 1225 (s), 1157 (s), 1097 (m), 1016 (w), 881 (w), 839 (s), 791 (m), 761 (w), 725 (w). Anal. calcd for $C_{70}H_{52}N_2$ (1291.69): C, 65.09; H, 4.06; N, 2.17. Found: C, 65.03; H, 3.87; N, 1.84.

(d) Ar = 2,4-{CH(4-FC$_6$H$_4$)$_2$}$_2$-6-EtC$_6$H$_2$ (Ni4). By employing a similar approach to that described for **Ni1** but using **L4** as the a-diimine, **Ni4** was isolated as a brick red complex (0.155 g, 78%). ^{19}F NMR (470 MHz, $CDCl_3$): δ −114.53, −115.38, −115.42, −116.45. FT-IR (cm^{-1}): 3046 (w), 2970 (w), 2875 (w), 1893 (w), 1641 (m, $\nu_{C=N}$), 1601 (m), 1505 (s), 1451 (w), 1415(w), 1376 (w), 1262 (w), 1225 (s), 1158 (s), 1097 (m), 1015 (w), 991 (w), 832 (s), 793 (m), 753 (w),719 (w), 702 (w). Anal. calcd for $C_{72}H_{56}N_2$ (1319.74): C, 65.53; H, 4.28; N, 2.12. Found: C, 65.70; H, 4.10; N, 2.05.

(e) Ar = 2,4-{CH(4-FC$_6$H$_4$)$_2$}$_2$-6-iPrC$_6$H$_2$ (Ni5). By employing a similar approach to that described for **Ni1** but using **L5** as the a-diimine, **Ni5** was isolated as a brick red complex (0.157 g, 78%). ^{19}F NMR (470 MHz, $CDCl_3$): δ −114.20, −115.30, −115.36, −116.73. FT-IR (cm^{-1}): 2963 (w), 2913 (w), 2873 (w), 1977(w), 1635 (m, $\nu_{C=N}$), 1602 (m), 1505 (s), 1451 (w), 1411 (w), 1379 (w), 1302 (w), 1225 (s), 1157 (s), 1096 (w), 1015 (w), 992 (w), 873 (s), 830(s), 793 (m), 750 (w), 724 (w), 676 (w). Anal. calcd for $C_{74}H_{60}N_2$ (1347.80): C, 65.95; H, 4.49; N, 2.08. Found: C, 65.51; H, 4.57; N, 1.83.

Procedure for ethylene polymerization

Ethylene polymerization at $P_{C_2H_4}$ = 1 atm. A specified amount of precatalyst was loaded into a 250 mL Schlenk tube, equipped with a stir bar, and the tube evacuated and back-filled with nitrogen twice and ethylene once. Under an ethylene atmosphere, toluene (30 mL) followed by a pre-determined amount of aluminum alkyl co-catalyst was added. The reaction mixture was then stirred at the required temperature at $P_{C_2H_4}$ = 1 atm for the designated time before the ethylene supply was disconnected and the vessel vented. The resulting mixture was then quenched with 15% hydrochloric acid in ethanol and the polymer filtered and finally dried at 50 °C for 8 h.

Ethylene polymerization at $P_{C_2H_4}$ = 5 or 10 atm. The ethylene polymerization process was carried out in a stainless-steel autoclave (250 mL) fitted with a pressure control system, temperature controller and mechanical stirrer. The autoclave was evacuated and backfilled with nitrogen three times and then with ethylene once. When the reactor had reached the desired reaction temperature, toluene (25 mL) and a solution of the nickel precatalyst dissolved in toluene (25 mL) were added successively. Then the required amount of co-catalyst (MAO, $EtAlCl_2$) and remaining toluene (50 mL) added. The mixture was then stirred at either $P_{C_2H_4}$ = 10 or 5 atm for the selected time. At the end of the run, the supply of ethylene was ceased, and the reactor vented. The resulting mixture was quenched with 15% solution hydrochloric acid in ethanol and filtered. After drying for 8 h at 50 °C under reduced pressure, the polymer was weighed.

X-ray crystallographic determinations

Single crystal X-ray diffraction studies on **L3**, **Ni1** and **Ni5** were performed on Rigaku-Axis fast IP diffractometer using graphite-monochromated Cu-Kα radiation (λ = 1.54184 Å) at 169.99 K. All hydrogen atoms were placed in calculated positions. The intensities were corrected for Lorentz polarization effects and empirical absorptions. The structures were solved by direct methods and refined by full-matrix least squares on F^2. Structure solution and refinement were undertaken using the SHELXL package.[42] Crystal data and crystallographic parameters for **L1**, **Ni1** and **Ni5** are summarized in Table S1.†

Conclusions

A series of novel 2,3-dimethyl-1,4-diazabutadienes (**L1–L5**) and their nickel(II) complexes (**Ni1–Ni5**), all bearing *para*-bis(4-fluorophenyl)methyl groups but differing in the *ortho*-substitution, have been successfully synthesized. Complex characterization has been achieved through FT-IR and NMR spectroscopy and in the case of **Ni1** and **Ni5** by single crystal X-ray diffraction; distorted tetrahedral geometries were a feature. With the addition of a *para*-fluoro substituents to the benzhydryl phenyl groups, the catalytic performance of these nickel complexes for ethylene polymerization has shown clear improvements. In particular, a positive influence on the thermal stability of the catalyst and the molecular weight of polyethylene was observed. Notably, this modification when applied to the *ortho*-substitution pattern has allowed access to high molecular weight polyethylenes displaying a high selectivity for short chain methyl branches. Indeed, this good control of the branching architecture has manifested itself in polyethylenes exhibiting promising elastomeric properties. A further notable feature of interest is that *ortho*-ethyl (**Ni2**, **Ni4**) had a beneficial influence on producing low molecular weight polyethylene.

Of particular note, **Ni5** on activation with EASC showed the highest activity of 1.0×10^7 g of PE per (mol of Ni) per h at 40 °C, while the polyethylene displayed not only a high molecular weight but also a high degree of branching (102 branches/1000 carbons: % Me = 87.7). Moreover, mechanical tests performed on these branched polyethylenes highlighted the role played by

crystallinity (X_c) and molecular weight (M_w) on the tensile strength (σ_b) and elongation at break (ε_b).

Conflicts of interest

There are no conflicts to declare.

Acknowledgements

This work was supported by the National Natural Science Foundation of China (No. 21871275). G. A. S. thanks the Chinese Academy of Sciences for a President's International Fellowship for Visiting Scientists. Y. M. thanks the Chinese Academy of Sciences for the support provided by a visiting scholarship to the UK.

Notes and references

1 (*a*) S. D. Ittel, L. K. Johnson and M. Brookhart, *Chem. Rev.*, 2000, **100**, 1169–1203; (*b*) V. C. Gibson, C. Redshaw and G. A. Solan, *Chem. Rev.*, 2007, **107**, 1745–1776; (*c*) Z. B. Guan and C. S. Popeney, *Top. Organomet. Chem.*, 2009, **26**, 179–220; (*d*) C. Bianchini, G. Giambastiani, L. Luconi and A. Meli, *Coord. Chem. Rev.*, 2010, **254**, 431–455; (*e*) T. Xiao, W. Zhang, J. Lai and W.-H. Sun, *C. R. Chim.*, 2011, **14**, 851–855; (*f*) H. Mu, L. Pan, D. Song and Y. Li, *Chem. Rev.*, 2015, **115**, 12091–12137; (*g*) F. Wang and C. Chen, *Polym. Chem.*, 2019, **10**, 2354.

2 (*a*) W. Zhang, W.-H. Sun and C. Redshaw, *Dalton Trans.*, 2013, **42**, 8988–8997; (*b*) J. Ma, C. Feng, S. Wang, K.-Q. Zhao, W.-H. Sun, C. Redshaw and G. A. Solan, *Inorg. Chem. Front.*, 2014, **1**, 14–34.

3 (*a*) R. Gao, W.-H. Sun and C. Redshaw, *Catal. Sci. Technol.*, 2013, **3**, 1172–1179; (*b*) S. Wang, W.-H. Sun and C. Redshaw, *J. Organomet. Chem.*, 2014, **751**, 717–741; (*c*) Z. Wang, Q. Liu, G. A. Solan and W.-H. Sun, *Coord. Chem. Rev.*, 2017, **350**, 68–83; (*d*) I. Soshnikov, K. Bryliakov, A. Antonov, W.-H. Sun and E. Talsi, *Dalton Trans.*, 2019, **48**, 7974–7984.

4 (*a*) L. K. Johnson, C. M. Killian and M. Brookhart, *J. Am. Chem. Soc.*, 1995, **117**, 6414–6415; (*b*) C. M. Killian, D. J. Tempel, L. K. Johnson and M. Brookhart, *J. Am. Chem. Soc.*, 1996, **118**, 11664–11665.

5 (*a*) M. Gasperini, F. Ragaini, E. Gazzola, A. Caselli and P. Macchi, *Dalton Trans.*, 2004, 3376–3382; (*b*) D. H. Camacho, E. V. Salo, J. W. Ziller and Z. Guan, *Angew. Chem., Int. Ed.*, 2004, **43**, 1821–1825; (*c*) D. Meinhard, M. Wegner, G. Kipiani, A. Hearley, P. Reuter, S. Fischer, O. Marti and B. Rieger, *J. Am. Chem. Soc.*, 2007, **129**, 9182; (*d*) K. E. Allen, J. Campos, O. Daugulis and M. Brookhart, *ACS Catal.*, 2014, **5**, 456; (*e*) S. Dai, X. Sui and C. Chen, *Angew. Chem., Int. Ed.*, 2015, **54**, 9948; (*f*) S. Zhong, Y. Tan, L. Zhong, J. Gao, H. Liao, L. Jiang, H. Gao and Q. Wu, *Macromolecules*, 2017, **50**, 5661; (*g*) F. Zhai and R. Jordan, *Organometallics*, 2017, **36**, 2784–2799; (*h*) J. Fang, X. Sui, Y. Li and C. Chen, *Polym. Chem.*, 2018, **9**, 4143–4149; (*i*) L. A. Brown, W. C. Anderson Jr, N. E. Mitchell, K. R. Gmernicki and B. K. Long, *Polymer*, 2018, **10**, 41; (*j*) L. Guo, Y. Liu, W. Sun, Q. Du, Y. Yang, W. Kong, Z. Liu and D. Chen, *J. Organomet. Chem.*, 2018, **877**, 12–20; (*k*) A. Vignesh, Q. Zhang, Y. Ma, T. Liang and W. Sun, *Polymer*, 2020, **187**, 122089; (*l*) S. Li and S. Dai, *Polym. Chem.*, 2020, **11**, 7199.

6 (*a*) C. M. Killian, L. K. Johnson and M. Brookhart, *Organometallics*, 1997, **16**, 2005–2007; (*b*) S. A. Svefda and M. Brookhart, *Organometallics*, 1999, **18**, 65–74; (*c*) D. P. Gates, S. A. Svejda, E. Onate, C. M. Killian, L. K. Johnson, P. S. White and M. Brookhart, *Macromolecules*, 2000, **33**, 2320.

7 M. Mitani, J. Mohri, Y. Yoshida, J. Saito, S. Ishii, K. Tsuru, S. Matsui, R. Furuyama, T. Nakano, H. Tanaka, S. Kojoh, T. Matsugi, N. Kashiwa and T. Fujita, *J. Am. Chem. Soc.*, 2002, **124**, 3327–3336.

8 (*a*) L. Fan, S. Du, C.-Y. Guo, X. Hao and W.-H. Sun, *J. Polym. Sci., Part A: Polym. Chem.*, 2015, **53**, 1369–1378; (*b*) Q. Mahmood, Y. Zeng, E. Yue, G. A. Solan, T. Liang and W.-H. Sun, *Polym. Chem.*, 2017, **8**, 6416–6430; (*c*) R. Wu, Y. Wang, R. Zhang, C.-Y. Guo, Z. Flisakb, Y. Sun and W.-H. Sun, *Polymer*, 2018, **153**, 574–586; (*d*) H. Suo, I. Oleynik, C. Huang, G. A. Solan, Y. Ma, T. Liang and W.-H. Sun, *Dalton Trans.*, 2017, **46**, 15684–15697; (*e*) S. Kong, C.-Y. Guo, W. Yang, L. Wang, W.-H. Sun and R. Glaser, *J. Organomet. Chem.*, 2013, **725**, 37–45; (*f*) Q. Mahmood, Y. Zeng, X. Wang, Y. Sun and W.-H. Sun, *Dalton Trans.*, 2017, **46**, 6934–6947; (*g*) X. Wang, L. Fan, Y. Ma, C.-Y. Guo, G. A. Solan, Y. Sun and W.-H. Sun, *Polym. Chem.*, 2017, **8**, 2785.

9 (*a*) R. Wu, Y. Wang, L. Guo, C.-Y. Guo, T. Liang and W.-H. Sun, *J. Polym. Sci., Part A: Polym. Chem.*, 2019, **57**, 130–145; (*b*) Y. Wang, A. Vignesh, M. Qua, Z. Wang, Y. Sun and W.-H. Sun, *Eur. Polym. J.*, 2019, **117**, 254–271; (*c*) S. Du, S. Kong, Q. Shi, J. Mao, C. Guo, J. Yi, T. Liang and W.-H. Sun, *Organometallics*, 2015, **34**, 582–590; (*d*) X. Wang, L. Fan, Y. Yuan, S. Du, Y. Sun, G. A. Solan, C.-Y. Guo and W.-H. Sun, *Dalton Trans.*, 2016, **45**, 18313; (*e*) R. Zhang, Z. Wang, Y. Ma, G. A. Solan, Y. Sun and W.-H. Sun, *Dalton Trans.*, 2019, **48**, 1878–1891; (*f*) Q. Zhang, R. Zhang, Y. Ma, G. A. Solan, T. Liang and W.-H. Sun, *Appl. Catal., A*, 2019, **573**, 73–86.

10 (*a*) H. Liu, W. Zhao, J. Yu, W. Yang, X. Hao, C. Redshaw, L. Chen and W.-H. Sun, *Catal. Sci. Technol.*, 2012, **2**, 415–422; (*b*) L. Fan, E. Yue, S. Du, C. Guo, X. Hao and W.-H. Sun, *RSC Adv.*, 2015, **5**, 93274–93282.

11 Y. Chen, S. Du, C. Huang, G. A. Solan, X. Hao and W.-H. Sun, *J. Polym. Sci., Part A: Polym. Chem.*, 2017, **55**, 1971–1983.

12 Q. Liu, W. Zhang, D. Jia, X. Hao, C. Redshaw and W.-H. Sun, *Appl. Catal., A*, 2014, **475**, 195.

13 Q. Mahmood and W.-H. Sun, *R. Soc. Open Sci.*, 2018, **5**, 180367.

14 L. Guo, W. Kong, Y. Xu, Y. Yang, R. Ma, L. Cong, S. Dai and Z. Liu, *J. Organomet. Chem.*, 2018, **859**, 58–67.

15 H. Rojas-Sáenz, G. V. Suárez-Moreno, I. Ramos-García, A. M. Duarte-Hernández, E. Mijangos, A. Peña-Hueso,

R. Contreras and A. Flores-Parra, *New J. Chem.*, 2014, **38**, 391–405.

16 (*a*) V. K. Voronov and I. A. Ushakov, *Russ. Chem. Rev.*, 2010, **79**, 835–847; (*b*) V. K. Voronov, I. A. Ushakov, S. N. Adamovich and E. N. Oborina, *Russ. Chem. Bull.*, 2021, **70**, 2354–2358.

17 Q. Zhang, Z. Li, M. Han, J. Xiang, G. A. Solan, Y. Ma and T. Liang W.-H. Sun, *Catal. Sci. Technol.*, 2021, **11**, 656–670.

18 M. G. Hogben and W. A. G. Graham, *J. Am. Chem. Soc.*, 1969, **91**(2), 283–291.

19 D. Jia, W. Zhang, W. Liu, L. Wang, C. Redshaw and W.-H. Sun, *Catal. Sci. Technol.*, 2013, **3**, 2737–2745.

20 J. L. Rhinehart, L. A. Brown and B. K. Long, *J. Am. Chem. Soc.*, 2013, **135**, 16316–16319.

21 M. Gao, S. Du, Q. Ban, Q. Xing, C. Redshaw and W.-H. Sun, *Organometallics*, 2015, **798**, 401–407.

22 H. Liu, W. Zhao, X. Hao, C. Redshaw, W. Huang and W.-H. Sun, *Organometallics*, 2011, **30**, 2418–2424.

23 (*a*) S. Yuan, T. Duan, R. Zhang, G. A. Solan, Y. Ma, T. Liang and W.-H. Sun, *Appl. Organomet. Chem.*, 2019, **33**, e4785; (*b*) S. Yuan, Z. Fan, Q. Zhang, Z. Flisak, Y. Ma, Y. Sun and W.-H. Sun, *Appl. Organomet. Chem.*, 2020, **34**, e5638; (*c*) M. Zada, L. Guo, R. Zhang, W. Zhang, Y. Ma, G. A. Solan, Y. Sun and W.-H. Sun, *Appl. Organomet. Chem.*, 2019, **33**, e4749.

24 C. Wen, S. Yuan, D. Liu, Q. Shi, E. Yue and W.-H. Sun, *Organometallics*, 2014, **33**, 7223–7231.

25 D. J. Tempel, L. K. Johnson, R. L. Huff, P. S. White and M. Brookhart, *J. Am. Chem. Soc.*, 2000, **122**, 6686.

26 J. Sun, F. Wang, W. Lia and M. Chen, *RSC Adv.*, 2017, **7**, 55051–55059.

27 X. Zhang, B. Duan, W.-H. Sun, S. Hsu and X. Yang, *Sci. China, Ser. B: Chem.*, 2009, **52**, 48–55.

28 Y. Chen, W. Yang, R. Sha, R.-D. Fu and W.-H. Sun, *Inorg. Chim. Acta*, 2014, **423**, 450–453.

29 W. Yang, Y. Chen and W.-H. Sun, *Macromol. Chem. Phys.*, 2014, **215**, 1810–1817.

30 G. Souza, F. Souza and B. J. Gusmao, *Appl. Catal., A*, 2007, **325**, 87–90.

31 R. S. Mauler, R. F. de. Souza, D. V. V. Vesccia and L. C. Simon, *Macromol. Rapid Commun.*, 2000, **21**, 458–463.

32 G. B. Galland, R. F. Souza, R. S. Mauler and F. F. Nunes, *Macromolecules*, 1999, **32**, 1620–1625.

33 (*a*) M. D. Leatherman, S. A. Svejda, L. K. Johnson and M. Brookhart, *J. Am. Chem. Soc.*, 2003, **125**, 3068–3081; (*b*) A. Michalak and T. Ziegler, *Organometallics*, 2003, **22**, 2069–2079; (*c*) L. Falivene, T. Wiedemann, I. Göttker-Schnetmann, L. Caporaso, L. Cavallo and S. Mecking, *J. Am. Chem. Soc.*, 2018, **140**, 1305–1312; (*d*) K. S. O'Connor, J. R. Lamb, T. Vaidya, I. Keresztes, K. Klimovica, A. M. LaPointe, O. Daugulis and G. W. Coates, *Macromolecules*, 2017, **50**, 7010–7027; (*e*) L. Pei, F. Liu, H. Liao, J. Gao, L. Zhong, H. Gao and Q. Wu, *ACS Catal.*, 2018, **8**, 1104–1113.

34 X. Luo, W. Huang and D. Yan, *J. Appl. Polym. Sci.*, 2016, **133**, 44127–44135.

35 X. Luo, S. Xie, J. H. Hu, J. Jiang, W. Huang, H. Gao, D. Zhou, Z. Lü and D. Yan, *Polym. Chem.*, 2014, **5**, 1305–1312.

36 Z. He, Y. Liang, W. Yang, H. Uchino, J. Yu, W.-H. Sun and C. C. Han, *Polymer*, 2015, **56**, 119–122.

37 S. Meiries, K. Speck, D. Cordes, A. Slawin and S. Nolan, *Organometallics*, 2013, **32**, 330–339.

38 P. Shaw, A. R. Kennedy and D. Nelson, *Dalton Trans.*, 2016, 1–3.

39 V. Lodeiro, T. Rosa, G. Aviles, B. Aullon and C. Covelo, *Inorg. Chem.*, 2008, **47**, 7734.

40 D. Zhang, E. Nadres, M. Brookhart and O. Daugulis, *Organometallics*, 2013, **32**, 5136.

41 K. V. Vasudevan, M. Findlater and A. H. Cowley, *Chem. Commun.*, 2008, **16**, 1918–1919.

42 (*a*) O. V. Dolomanov, L. J. Bourhis, R. J. Gildea, J. A. K. Howard and H. Puschmann, *J. Appl. Cryst.*, 2009, **42**, 339–341; (*b*) G. M. Sheldrick, *Acta Cryst.*, 2015, **A71**, 3–8; (*c*) G. M. Sheldrick, *Acta Cryst.*, 2015, **C71**, 3–8.